

Size dependent hygroscopicity of levoglucosan and D-glucose aerosol nanoparticles

Ting Lei^{1,2}, Hang Su^{2,3}, Nan Ma⁴, Ulrich Pöschl², Alfred Wiedensohler⁵, Yafang Cheng¹

¹Minerva Research Group, Max Planck Institute for Chemistry, 55128 Mainz, Germany

²Multiphase Chemistry Department, Max Planck Institute for Chemistry, 55128 Mainz, Germany

³State Environmental Protection Key Laboratory of Formation and Prevention of Urban Air Pollution Complex, Shanghai Academy of Environmental Sciences, Shanghai 200233, China

⁴Institute for Environmental and Climate Research, Jinan University, 511443 Guangzhou, China

⁵Leibniz Institute for Tropospheric Research, 04318 Leipzig, Germany

Correspondence to: Yafang Cheng (yafang.cheng@mpic.de)

Abstract: The interaction between water vapor and aerosol nanoparticles is important in atmospheric processes. Hygroscopicity of sub-10 nm organic nanoparticles and their concentration-dependent thermodynamic properties (e.g., water activity) in the highly supersaturated concentration range are, however, scarcely available. Here we investigate the size dependence of hygroscopicity of organics (i.e., levoglucosan, D-glucose) in dry particle diameter down to 6 nm using a nano-hygroscopicity tandem differential mobility analyzer (nano-HTDMA). Our results show that there is only a weak size dependent hygroscopic growth of both levoglucosan and D-glucose nanoparticles with diameters down to 20 nm. In the diameter range smaller than 20 nm (down to 6 nm), we observed a strong size-dependent hygroscopic growth for D-glucose nanoparticles. The hygroscopic growth factors cannot be determined for levoglucosan below 20 nm due to its evaporation. In addition, we compare hygroscopicity measurements for levoglucosan

删除了: The interaction between water vapor and aerosol nanoparticles is of great significance in atmospheric processes. However, current knowledge of hygroscopicity of sub-10 nm organic nanoparticles and their concentration-dependent thermodynamic properties (e.g., water activity) in the highly supersaturated concentration range is scarcely available. In this study, we investigate the size dependence of hygroscopicity of organics (i.e., levoglucosan, D-glucose) in size down to 6 nm using a nano-hygroscopicity tandem differential mobility analyzer (nano-HTDMA). There is a weak size dependence of the hygroscopic growth factor observed for levoglucosan and D-glucose nanoparticles with diameters down to 20 nm. However, a clear size-dependent hygroscopic growth factor is observed for D-glucose nanoparticles down to 6 nm in size. A reduction in diameters of sub-20 nm levoglucosan is observed at the dry RHs, which is explained by partial levoglucosan evaporation into gas phase, indicating high impact of volatility of sub-20 nm levoglucosan aerosol nanoparticles. However, this also means that the hygroscopic growth factors of levoglucosan nanoparticles with diameters below 20 nm are not possible to be determined. The use of water activity parameterization models proposed by Kreidenweis et al. (2005) (KD, Köhler), the Extend-Aerosol Inorganic Model (E-AIM (standard UNIFAC), and Differential Köhler Analysis (DKA) method is to determine thermodynamic properties (e.g., water activity) of levoglucosan and D-glucose nanodroplets as a function of solute concentration, respectively. Predicated water activity for these aqueous organic solutions (i.e., levoglucosan, D-glucose) from the different methods are similar to observations from references in the low solute concentration ($< 20 \text{ mol kg}^{-1}$), while a quite difference is found in the high solute concentration ($> 20 \text{ mol kg}^{-1}$). In addition, we compare hygroscopicity measurements for levoglucosan and D-glucose nanoparticles with the E-AIM (standard UNIFAC), the ideal solution theory, and DKA predictions, respectively. The ideal solution theory describes well the measured hygroscopic growth factors of levoglucosan with diameters down to 20 nm and D-glucose nanoparticles with diameters higher than 60 nm, respectively, while the E-AIM (standard UNIFAC) model can successfully predict the growth factors of levoglucosan with diameters from 100 down to 6 nm at RH above 88-40 % (e.g., at RH above 88 % for 100 nm D-glucose, at RH above 40 % for 6 nm D-glucose). The use of the DKA method leads to a good agreement with measured hygroscopic growth factors of D-glucose aerosol nanoparticles with diameters from 100 down to 6 nm.

设置了格式: 字体颜色: 文字 1

and D-glucose nanoparticles with the E-AIM (standard UNIFAC), the ideal solution theory, and DKA predictions, respectively. The ideal solution theory describes well the measured hygroscopic growth factors of levoglucosan with diameters down to 20 nm and D-glucose nanoparticles with diameters higher than 60 nm, respectively, while the E-AIM (standard UNIFAC) model can successfully predict the growth factors of D-glucose nanoparticles with diameters from 100 down to 6 nm at RH above 88-40 % (e.g., at RH above 88 % for 100 nm D-glucose, at RH above 40 % for 6 nm D-glucose). The use of the DKA method leads to a good agreement with measured hygroscopic growth factors of D-glucose aerosol nanoparticles with diameters from 100 down to 6 nm. Predicted water activity for these aqueous organic solutions (i.e., levoglucosan, D-glucose) from different parameterization methods agrees well with observations in the low solute concentration range ($< 20 \text{ mol kg}^{-1}$), and start to deviate from observations in the high solute concentration ($> 20 \text{ mol kg}^{-1}$).

设置了格式: 字体颜色: 自动设置, (中文) 中文(简体, 中国大陆)

删除了:

1 Introduction

Organic aerosol nanoparticles play an important role in new particle formation, subsequent condensation and coagulation growth, cloud condensation nuclei (CCN), and thus in affecting visibility degradation, radiative forcing, and climate (Chylek and Coakley, 1974; Charlson et al., 1992; Dusek et al., 2010; Cheng et al., 2012; Zhang et al., 2012; Kulmala et al., 2013). Both growth of nanoparticles and their ability to act as CCN are directly related to its hygroscopicity that describes the interaction between organic nanoparticles and water vapor (Köhler, 1936; Kreidenweis et al., 2005; Su et al., 2010; Cheng et al., 2015; Wang et al., 2015). However, current knowledge of hygroscopicity of sub-10 nm organic nanoparticles and their concentration-

96 dependent thermodynamic properties (e.g., water activity) in the highly supersaturated
97 concentration range is scarcely available.

98 Levoglucosan aerosol nanoparticles have attracted increasing interest in recent years (Simoneit et
99 al., 1999; Mochida and Kawamura, 2004; Mikhailov et al., 2009; Elias et al., 2010; Lei et al., 2014,
100 2018; Bhattarai et al., 2019) due to relative stability and high emission factors, which are

101 considered as an ideal tracer for characterization and quantification the biomass burning (Fraser

102 and Lakshmanan, 2000). Also, levoglucosan is typically the most abundant species in wood

103 burning aerosols, which contributes substantially (16.6–30.9% by mass) to the total organics in

104 PM_{2.5} (Mochida and Kawamura, 2004; Bhattarai et al., 2019). D-glucose, a hydrolysis product of

105 cellulose and levoglucosan, is a major pyrolysis product of wood (Mochida and Kawamura, 2004;

106 Bhattarai et al., 2019; Mikhailov and Vlasenko., 2020). Hygroscopicity of levoglucosan and D-

107 glucose substances is thus important in reproducing the overall hygroscopic behavior of the real

108 biomass burning aerosol particles (Bhandari and Bareyre. 2003; Mochida and Kawamura, 2004;

109 Chan et al., 2005; Koehler et al., 2006; Peng et al., 2010; Mikhailov and Vlasenko., 2020). For

110 example, a small difference in the hygroscopicity parameter (κ) between measured data of model

111 mixtures including levoglucosan and ammonium sulfate in the laboratory using HTDMA and

112 biomass burning aerosol particles in the field using CCN activity measurement due to the similar

113 O: C ratios of levoglucosan and ammonium sulfate mass fractions used in model mixtures when

114 experimental κ data from sub- and supersaturated water vapor conditions are compared (Bhandari

115 and Bareyre. 2003; Mochida and Kawamura, 2004; Chan et al., 2005; Koehler et al., 2006; Peng

116 et al., 2010; Pöhlker et al., 2016; Lei et al., 2018; Mikhailov and Vlasenko., 2020). Most of the

117 previous lab studies have focused on investigation of the hygroscopic behavior of 100-nm

118 levoglucosan and D-glucose aerosol nanoparticles, which mainly utilized the humidified tandem

119 differential mobility analyzers (DMAs) (Mikhailov et al., 2004; Mochida and Kawamura. 2004;

删除了: quantitation

设置了格式: 字体颜色: 文字 1

删除了: Also, levoglucosan is typically the most abundant species in wood burning aerosols, which contributes substantially (16.6–30.9% by mass) to the total organics in PM_{2.5} (Mochida and Kawamura, 2004). D-glucose, a hydrolysis product of cellulose and levoglucosan, is a major pyrolysis product of wood (Mochida and Kawamura, 2004). Levoglucosan and D-glucose substances may be representative in reproducing the hygroscopic behavior of the real biomass burning aerosol particles (Bhandari and Bareyre. 2003; Mochida and Kawamura, 2004; Chan et al., 2005; Koehler et al., 2006; Peng et al., 2010).

设置了格式: 字体颜色: 文字 1

删除了: been

133 Koehler et al., 2006; Lei et al., 2014; 2018). For example, Mochida and Kawamura (2004) observed
134 that 100-nm levoglucosan and D-glucose aerosol nanoparticles uptake/release water continuously
135 in both deliquescence and efflorescence modes, respectively. To our knowledge, there are no phase
136 transitions for these organic aerosol nanoparticles in both deliquescence and efflorescence
137 processes.

删除了: hydration

删除了: dehydration

138 Early studies showed that the hygroscopicity and solubility of inorganic aerosols, such as
139 ammonium sulfate (AS) and sodium chloride (NaCl), exhibited a strong size dependence (Cheng
140 et al., 2015). Firstly, hygroscopic diameter growth factors of AS, NaCl as well as Na₂SO₄
141 nanoparticles are found to decrease with size decreases in both deliquescence and efflorescence
142 modes (Biskos et al., 2006a, b, c, Lei et al., 2020). Secondly, there is no significant difference in
143 the deliquescence relative humidity (DRH) and the efflorescence relative humidity (ERH) between
144 AS nanoparticles with dry diameters of 6 and 60 nm (Biskos et al., 2006b; Lei et al., 2020), while
145 a pronounced size dependence of the DRH of NaCl is up to 10 % RH between dry diameters of 6
146 and 60 nm (Biskos et al., 2006a). The behaviors of change of phase transition RH and
147 concentrations of Na₂SO₄ are between NaCl and AS (Lei et al., 2020). However, there are very few
148 lab studies on investigating hygroscopicity (g_f , DRH, ERH) of organic aerosol nanoparticles in sub-
149 10 nm size range (Wang et al., 2017). It is not clear how the size effect influences the hygroscopic
150 growth of organics, especially those without DRH and ERH. Besides technique limitation (Lei et
151 al., 2020; Wang et al., 2017), another reason is the high diffusion of sub-100 nm organic
152 nanoparticles, especially in the sub-10 nm size range, which results in nanoparticle losses in the
153 HTDMA system (Seinfeld and Pandis, 2006).

删除了: is going to

删除了: with no

删除了: s

删除了: For inorganic aerosols, the lack of thermodynamic properties of the highly supersaturated aqueous solution nanodroplets (Tang and Munkelwitz, 1994; Tang 1996; Pruppacher and Klett, 1997; Clegg et al., 1998) are limiting predictability of aerosol hygroscopic behavior of sub-10 nm aerosol nanoparticles (Cheng et al., 2015). Also, there are very few thermodynamic data in the highly supersaturated concentration for organic solution, such as levoglucosan and D-glucose (Bhandari and Bareyre. 2003; Chan et al., 2005; Koehler et al., 2006; Peng et al., 2010). By measuring the hygroscopic growth factor of particles of different sizes, we may be able to retrieve these thermodynamic data using a Differential Köhler Analysis (DKA) method (Cheng et al., 2015). This will further help us to understand the new particle formation, transportation, and their interactions between water molecules.

154 Thermodynamic model is widely used to predict the hygroscopic growth factor of organic aerosol
155 particles as a function of RH (Bhandari and Bareyre. 2003; Chan et al., 2005; Koehler et al., 2006;

Peng et al., 2010). The thermodynamic model needs thermodynamic data such as water activity, liquid-vapor interfacial energy (surface tension), and density of organic aqueous solutions (Tang and Munkelwitz, 1994; Tang 1996; Pruppacher and Klett, 1997; Clegg et al., 1998). Because nanodroplets can become more highly supersaturated where no thermodynamic data are available, it makes the current thermodynamic model difficult or impossible to predict the hygroscopic behavior of organic aerosol nanoparticles. Cheng et al. (2015) pointed out that size effect might be taken models into account. By measuring the hygroscopic growth factor of organic nanoparticles (e.g., levoglucosan and D-glucose) of different sizes, we may be able to retrieve these thermodynamic data using a Differential Köhler Analysis (DKA) method (Cheng et al., 2015). This will further help us to understand the new particle formation, transportation, and their interactions between water molecules.

In this study, we investigate the hygroscopic growth factors of levoglucosan and D-glucose nanoparticles in size down to 6 nm using a nano-hygroscopic tandem differential mobility analyzer (nano-HTDMA, Lei et al., 2020). Moreover, we compare our measurement data with model prediction from the Extended Aerosol Inorganic Model (E-AIM (standard UNIFAC)) (Clegg et al., 2001; Clegg and Seinfeld, 2006; available online: <http://www.aim.env.ac.uk/aim/aim.php>), the ideal solution theory, and DKA. In addition, the use of the DKA method is to calculate thermodynamic properties (e.g., water activity) of D-glucose nanodroplets in the highly supersaturated concentration range and then to compare with KD-derived data (KD=Kreidenweis), thermodynamic property data from Köhler (Kreidenweis et al., 2005), E-AIM (standard UNIFAC) model, and references, respectively.

2 Methodology

200 2.1 Experimental methods

201 2.1.1 Nanoparticle generation

202 An electrospray is employed to generate levoglucosan and D-glucose aerosol nanoparticles of 6, 8,
203 10, and 15 nm using 2, 3, 5, and 10 mM aqueous solutions with 50 % volume fraction of a 20 mM
204 ammonium acetate buffer solution (Chen et al., 2005; Wang et al., 2015), respectively. The
205 generated nanoparticles are diluted by mixing with dry and filtered N₂ (1 l/min) and CO₂ (0.1 l/min),
206 bringing aerosol nanoparticles to a dry RH state ($\leq 2\%$ RH). Subsequently, aerosol nanoparticles
207 pass through a Po²¹⁰ neutralizer to reach the equilibrium charge distribution (Wiedensohler 1986).
208 In order to avoid blocking the 25- μ m capillary tube in the electrospray with high solution
209 concentration, the aerosol nanoparticles with diameters of 60-100 and 20 nm are generated by an
210 atomizer with a 0.05 and 0.01 wt % organic solution (i.e., levoglucosan and D-glucose),
211 respectively. The chemical substances and their physical properties are characterized in Table S1.
212 These solutions are prepared with distilled and de-ionized million-Q water (resistivity of 18.2 M Ω
213 cm at 298.15 K). Note that, the size selected by the nano-DMA1 should be the right part of peak
214 diameter of the number size distribution of the generated nanoparticles, which minimizes the
215 influence of the multiple charged nanoparticles in hygroscopicity measurements. This is to ensure
216 that we could have as many particles as possible to compensate for the strong loss of very small
217 particles in the whole humidification system.

设置了格式: 字体颜色: 文字 1

设置了格式: 字体颜色: 文字 1

218 2.1.2 Nano-HTDMA setup

219 Figure 1 shows a schematic of the nano-HTDMA system for investigating the hygroscopic
220 behavior of aerosol nanoparticles, especially in the sub-10 nm size range. The detailed description,
221 calibration, and validation of nano-HTDMA setup have been reported in the previous paper (Lei et
222 al., 2020). In brief, the polydisperse aerosol nanoparticles pass through a silica gel diffusion dryer

and a Nafion gas dryer (TROPOS Model ND.070, Length 60 cm). The dry aerosol nanoparticles at RH below 10 % are charged by a Kr⁸⁵ bipolar charger and then enter the first nano-differential mobility analyzer (nano-DMA1, TROPOS Model Vienna-type short DMA), where a monodisperse distribution of nanoparticles with the desired dry diameter is selected. The monodispersed nanoparticles subsequently are exposed to the different RH conditions, which can be set to deliquescence mode (from low RH to high RH for measuring deliquescence) or efflorescence mode (from the high RH to low RH for measuring efflorescence). In the deliquescence mode, the dry aerosol nanoparticles are gradually humidified to a target RH through a Nafion humidifier (NH-1, TROPOS Model ND.070, Length 60 cm). In the efflorescence mode, after deliquescence of aerosol nanoparticles with RH above 97% in a Nafion humidifier (NH-2: Perma Pure Model MH-110, Length 30 cm), the deliquesced aerosol nanoparticles are stepwise dried to a target RH in NH-1. The number size distribution of the humidified nanoparticles is then measured by a nano-differential mobility analyzer (nano-DMA2) at a target RH through a Nafion humidifier (NH-3, Perma Pure Model PD-100) coupled with an ultrafine condensation particle counter (CPC, TSI, model no. 3776). To have the uniform RH within the nano-DMA2 for the accurate determination of hygroscopicity (g_f , DRH, ERH) of aerosol nanoparticles, the difference between the sheath flow RH (RH_s) and the aerosol flow RH (RH_a) upstream of the nano-DMA2 is kept <1 %. Most importantly, the temperature difference between inlet and outlet of the nano-DMA2 is maintained below 0.2 °C during the measurements. In addition, the residence time (e.g., 5.4 s: between the humidifier and the nano-DMA2; 0.07 s: deliquescence for aerosol nanoparticles) is sufficient for water-soluble aerosol nanoparticles to equilibrate with water vapor at a given RH and to occur solid-liquid phase transition (Kerminen 1997; Duplissy et al., 2005; Raoux et al., 2007), respectively.

2.2 Theory and modeling methods

247 2.2.1 Köhler theory

248 The fractional ambient relative humidity ($\frac{RH}{100}$) over a spherical droplet in equilibrium with the
249 environment is described by Köhler equation (Köhler 1936):

$$250 \frac{RH}{100} = a_w \exp\left(\frac{4\sigma_{sol}v_w}{RTG_fD_s}\right) \quad (1)$$

251 where a_w is the water activity of the solution droplet, σ_{sol} is the liquid-vapor interfacial energy of
252 solution droplet (also called surface tension), v_w is the partial molar volume of water, R is the
253 universal gas constant, T is the temperature, G_f is the diameter growth factor of aerosol particles,
254 and D_s is the dry diameter of spherical aerosol particles. The hygroscopic growth curve (G_f vs RH)
255 is estimated based on the assumptions in models or theories described in the following sections
256 (2.2.2-2.2.3).

257 2.2.2 Water activity

258 The expression for water activity used in the simplified Köhler theory assumes the droplet contains
259 n_w moles of water and n_s moles of nonvolatile solute.

$$260 a_w = \frac{n_w}{n_w + vn_s} \quad (2)$$

261 v is the number of ions of solute present in solution ($v=1$ for organic composition). This expression
262 has been applied to the diluted solution (Kreidenweis et al., 2005; Koehler et al., 2006).

263 The following KD expression proposed by Kreidenweis et al. (2005) (KD= Kreidenweis) is to
264 present the relationship between a_w and G_f determined in hygroscopic growth measurements:

$$265 Gf = \left[1 + (a + b * a_w + c * a_w^2) \frac{a_w}{1-a_w}\right]^{\frac{1}{3}} \quad (3)$$

删除了:
2.2.2.1 Köhler

删除了:
2.2.2.2 KD

删除了: is

271 The coefficients a, b, and c for organic solution droplet in this study from Lei et al. (2014, 2018)
272 and Estillore et al. (2017) as shown in Table S2.

273 Differential Köhler analysis (DKA) proposed by Cheng et al. (2015) is theoretically based on
274 Köhler equation (Köhler, 1936) to determine water activity by measuring hygroscopic growth
275 factors of aerosol nanoparticles in different sizes.

$$276 \quad a_w = \frac{s_{w1}^{\left(\frac{D_{s1}}{D_{s1}-D_{s2}}\right)}}{s_{w2}^{\left(\frac{D_{s2}}{D_{s1}-D_{s2}}\right)}} \quad (4)$$

277 where s_{w1} and s_{w2} are water saturation ratio measured at the same g_f but at the different initial dry
278 diameters (D_{s1}, D_{s2}), respectively. Using the DKA method can calculate the water activity in the
279 highly supersaturated concentration range.

280 2.2.3 Growth factor

281 For ideal solution, the hygroscopic curve can be estimated assuming that the water activity a_w of
282 the solution containing non-volatile and non-electrolyte solute component is equal to the molar
283 ratio of water in the solution. Here, the partial molar volume of pure water in the solution is equal
284 to the molar volume of pure water. Since the hygroscopic diameter growth factor measurements
285 are on volume basis using nano-HTDMA system, the expression of G_f as a function of molar ratio
286 (x_j), molar mass (M_j), and mass density (ρ_j) of components j as follows:

$$287 \quad G_f = \left[\frac{\sum_j \left(x_j M_j^{\frac{1}{\rho_j}} \right)}{\sum_{j,j \neq w} \left(x_j M_j^{\frac{1}{\rho_j}} \right)} \right]^{\frac{1}{3}} \quad (5)$$

288 The hygroscopic growth curve of aerosol particles is commonly evaluated from Extend-Aerosol
289 Inorganic Model (E-AIM). It is a thermodynamic equilibrium model used for calculating phase
290 partitioning (gas/liquid/solid). Most importantly, the E-AIM mode can model thermodynamic

删除了: 2.2.2.3 DKA

删除了: $A = \frac{4v_w}{RTg_f}$,

删除了: 2.2.3.1 Ideal solution growth factor

删除了: 2.2.3.2 Growth factor prediction by E-AIM model

properties (e.g., water activity, liquid-vapor interfacial energy, and solution density) in the highly supersaturated concentration solution (Dutcher et al., 2013). Also, the standard universal quasi-chemical functional group activity coefficients (UNIFAC) within E-AIM can be used to predict a_w , σ_{sol} , and ρ_{sol} of organic aqueous solution (Fredenslund et al., 1975; Hansen et al., 1991). Note that ~~that~~. The E-AIM calculations based on the standard UNIFAC group contribution method are to predict hygroscopic growth factors of organic aerosol particles. (i.e., E-AIM model (standard UNIFAC)) growth curve as a function of RH is based on Eq. (1) and Eq. (6).

$$G_f = \left(\frac{\rho_s}{x_s \rho_{sol}} \right)^{\frac{1}{3}} \quad (6)$$

ρ_s and ρ_{sol} are the density of solute and solution, respectively, and x_s is the solute mass fraction.

3 Results and discussion

3.1 Levoglucosan

3.1.1 Concentration-dependent water activity of levoglucosan solution

By applying a water activity parameterization model (KD, Eq. 3) to measured growth factors of levoglucosan aerosol nanoparticles with diameters from 20 to 100 nm using a nano-HTDMA, as shown in Fig. 2, we obtain water activity of aqueous levoglucosan nanoparticles with molality up to 140 mol kg⁻¹. Chan et al. (2005) levitated single particles of ~10 μm levoglucosan at the different RHs in an electrodynamic balance for mass measurements, and reported water activity data for aqueous droplets with molality up to 14 mol kg⁻¹. These water activity data are compared with predictions from the Köhler (Kreidenweis et al., 2005, Eq. 2) and the E-AIM model, respectively. A good agreement between KD-derived water activity and Köhler indicates these aerosol particles are diluted aqueous droplets with molality less than 20 mol kg⁻¹. However, a derivation of Köhler

删除了: .

删除了: 2.2.4 Calculation of ratio of gas-phase concentration to the total concentration

删除了: 2.2.4.1 Calculation of gas-phase concentration (g/cm³)

$$P_A = P_A^0 \exp \left(\frac{2\sigma M}{RT \rho_l R_p} \right) \quad (7)$$

$$m_{gas} = \frac{PVM}{RT} \quad (8)$$

where P_A and P_A^0 are vapor pressure, equilibrium vapor pressure, respectively. σ , M , ρ_l , and R_p mean surface tension, molecular weight of the substance, liquid-phase density, and a droplet of radius, respectively. This equation (Eq. 8) establish a relationship between mass in gas phase (m_{gas}) and pressure (P), volume (V), mole mass (M), the ideal gas constant (R), and temperature. Here, Vapor pressure (P) is equal to saturated ratio of levoglucosan vapor multiplied saturated levoglucosan vapor pressure at 293.15 K.

2.2.4.2 Calculation of total concentration of generated particles (g/cm³)

$$m_{total} = \frac{dN}{d \log D_p} \times d \log D_p \times \frac{\pi}{6} D_p^3 \times \rho \quad (9)$$

where dN is particle concentration, D_p is the particle diameter, and ρ is the density of particles.

2.2.4.3 Ratio of the gas-phase concentration to the total concentration of generated particles

$$Ratio = \frac{m_{gas}}{m_{total}} \quad (10)$$

设置了格式: 字体颜色: 文字 1

删除了: Figure 2 shows KD-derived water activity of aqueous levoglucosan nanoparticles with molality up to 140 mol kg⁻¹. Here, by applying a water activity parameterization model (KD, Eq. 3) to measured growth factors of levoglucosan aerosol nanoparticles with diameters from 20 to 100 nm using a nano-HTDMA.

from the KD-derived water activity is observed as the molality increases from 20 to 120 mol kg⁻¹, indicating levoglucosan nanoparticles become highly supersaturated. Also, a discrepancy exists between KD-derived data and E-AIM model prediction. For DKA-derived water activity calculations, a strong size dependence of the hygroscopic growth factors is needed for aerosol nanoparticles in the different sizes, which is not the case for the hygroscopic measurements of levoglucosan nanoparticles.

3.1.2 Size dependent hygroscopicity of levoglucosan nanoparticles

Black solid squares in Fig. 3 shows the measured humidogram of 100-nm levoglucosan nanoparticles in both deliquescence and efflorescence modes. Levoglucosan nanoparticles uptake water continuously from 5 % to 90 % RH. Also, they gradually release water as RH decreases down to 5 %. The hygroscopic growth factors of levoglucosan nanoparticles in deliquescence and efflorescence modes overlap. For example, the hygroscopic growth factors of levoglucosan nanoparticles at 80 % RH, 87 % RH are 1.16, 1.23, respectively, in the deliquescence mode, very close to the corresponding values in the efflorescence mode are 1.15, 1.22 (shown in Fig. S1), suggesting that growing and shrinking of particles are in equilibrium with water vapor surrounding moisture conditions. No prompt phase transitions of levoglucosan nanoparticles are observed in both deliquescence and efflorescence modes. A similar non-prompt phase transition of levoglucosan nanoparticles was observed in the previous studies (Mochida and Kawamura, 2004; Chan et al., 2005; Svenningsson et al., 2006; Mikhailov et al., 2008; Lei et al., 2014, 2018). This study is in good agreement with most of reference results, but there is a difference in the hygroscopic growth factor of levoglucosan nanoparticles between Mikhailov et al. (2008) and this study. The reason is that Mikhailov et al. (2008) used minimum mobility diameter measured in the deliquescence and efflorescence modes instead of the initial dry mobility diameter measured in the

删除了: the

删除了: hydration

删除了: dehydration

379 ~~deliquescence~~ or ~~efflorescence~~ modes to calculate the hygroscopic growth factor of levoglucosan
380 nanoparticles, which could lead to the higher hygroscopic growth factors of levoglucosan
381 nanoparticles than ~~those~~ of this study.

删除了: hydration

删除了: dehydration

删除了: at

382 Figure 4 shows measured size-resolved hygroscopic growth factors of levoglucosan nanoparticles
383 against RH up to 90 %. There is a weak size dependence of hygroscopic growth factors of
384 levoglucosan nanoparticles with diameters down to 20 nm in both deliquescence and efflorescence
385 modes. E.g., a slight difference in hygroscopic growth factor between 100 and 20-nm levoglucosan
386 nanoparticles is ~0.02 at 88 % RH. In addition, E-AIM (standard UNIFAC) model and ideal
387 solution theory are used to predict our measurement results as shown in Fig. 4a and 4b, respectively.
388 E-AIM (standard UNIFAC) model is applied to estimate the hygroscopic growth of organic aerosol
389 nanoparticles according to UNIFAC group contribution method. Ideal solution theory is used to
390 describe water absorption of the ideal/diluted aqueous solution nanodroplets. Due to consideration
391 of Kelvin effect in model and theory, these model predictions are expected to present a size
392 dependence of growth factors of nanoparticles in size from 100 down to 20 nm. For example, as
393 shown in Fig. 4a, the thermodynamic equilibrium model (E-AIM (standard UNIFAC)) shows a
394 weak size dependence of the growth factors of levoglucosan nanoparticles with diameters 100, 60,
395 and 20 nm at low RH but a strong size dependence of growth factors at RH above 70 %. However,
396 the calculated growth factors of nanoparticles down to 20 nm in size are deviated from the
397 measured growth factors of levoglucosan nanoparticles at RH below 80 %, which is similar to the
398 observation of 100-nm levoglucosan hygroscopicity prediction from previous studies (Lei et al.,
399 2014, 2018). Lei et al. (2014, 2018) explained that the possible reason for this discrepancy is that
400 the E-AIM (standard UNIFAC) predictions are not suitable for organic compounds with the
401 strongly polar functional groups in series (Fredenslund et al., 1975; Hansen et al., 1991). Since
402 levoglucosan contains three OH groups in series, thus, thermodynamic properties (e.g., water

activity, surface tension) in E-AIM (standard UNIFAC) are more likely to be invalid for levoglucosan system. However, a good agreement of growth factors of levoglucosan with diameters 100, 60, and 20 nm is observed between measurements and predictions by ideal solution theory as shown in Fig. 4b.

The hygroscopic growth for sub-20 nm levoglucosan nanoparticles cannot be determined with the nano-HTDMA system because we observed significant evaporation of the dry particles in the measurement system. Figure 5a-b shows the measured peak diameter of normalized size distribution scanned by the nano-DMA2 and nano-DMA1 for sub-20 nm levoglucosan nanoparticles. It is obvious that the size of nanoparticles in DMA2 is smaller than that in DMA1, corresponding to a decrease of 22% to 50% of 15-nm and 10-nm levoglucosan nanoparticles, respectively, indicating significant evaporation of these small levoglucosan nanoparticles in the system. To test this hypothesis, we estimate the ratio of gas-phase concentration to the total concentration of the generated levoglucosan nanoparticles in the different sizes. Firstly, the calculated gas-phase concentration of levoglucosan is based on the Kelvin equation and ideal gas equation (Eq. [S1&S2](#), [SI. S1](#)). Figure 5c shows the vapor saturation ratio of levoglucosan as nanodroplet diameter increases from 0 to 100 nm. The inset in Fig. 5c is an enlarged view (black open square) of vapor saturation ratio of levoglucosan as a function of nanodroplet diameters below

20 nm. Levoglucosan is semi-volatile at ambient condition (Hennigan et al., 2010). Due to Kelvin effect, sub-20 nm levoglucosan aerosol particles become more volatile. Secondly, the total concentration of levoglucosan particles is estimated by Eq. ([S3](#)). Thus, the results of the ratio of gas-phase concentration (m_g) to the total concentration (m_t) have been shown in Fig. 5d and Table S3 for levoglucosan nanoparticles in the diameter range from 10 to 100 nm. It shows a slight increase in the calculated ratio (m_g/m_t) for levoglucosan aerosol nanoparticles with dimeters from 100 down to 20 nm. However, the ratio of gas-phase concentration to the total concentration is

删除了: 7

删除了: 8

删除了: Sect. 2.2.4

设置了格式: 字体颜色: 文字 1

删除了: The Kelvin effect on levoglucosan nanodroplets is very weak at diameters above 20 nm, but significantly enhanced for levoglucosan nanodroplets with diameters below 20 nm.

删除了: 9

dramatically enhanced for sub-20 nm levoglucosan aerosol nanoparticles, which is consistent with measurement observations, indicating the larger impact of evaporation of sub-20 nm levoglucosan nanoparticles on the measurement results. Therefore, there is an obvious partial levoglucosan evaporation from DMA1 to DMA2 within several seconds.

设置了格式: 字体颜色: 文字 1

3.2 D-glucose

3.2.1 Concentration-dependent water activity of D-glucose solution

Figure 6 shows the DKA-derived water activity of aqueous D-glucose nanodroplets with diameters from 6 nm to 100 nm with molality up to 1000 mol kg⁻¹ (Cheng et al., 2015, Eq. 4). Here, by comparing with KD-derived water activity, Köhler, E-AIM model, and observation from literatures (Comesaña et al., 2001; Peng et al., 2001; Bhandari and Bareyre, 2003; Ferreira et al., 2003), a good agreement among them is observed in the solute concentration below 20 mol kg⁻¹. However, there is a disagreement between water activity results in the highly supersaturated concentration range (> 20 mol kg⁻¹).

删除了: between

3.2.1 Size dependent hygroscopicity of D-glucose nanoparticles

Figure 7 shows the measured hygroscopic growth factors of 100-nm D-glucose nanoparticles as a function of RH. No significant difference in the hygroscopic growth factor of 100-nm D-glucose nanoparticles is found between deliquescence and efflorescence measurement modes (Fig. S2). For example, the measured growth factors of D-glucose nanoparticles at 81 % RH, 88 % RH are 1.16, 1.25 in the deliquescence mode, respectively, in good agreement with results in the efflorescence mode ($g_f=1.17$ at 81 % RH, $g_f=1.26$ at 88 % RH shown in Fig. S2). Also, measured hygroscopic growth factors of 100-nm D-glucose are consistent with results from previous studies (Mochida and Kawamura, 2004; Chan and Chan, 2005; Suda and Petters, 2013; Estillore et al., 2017;

设置了格式: 字体颜色: 文字 1

Mikhailov and Vlasenko, 2020). For example, Mikhailov and Vlasenko, (2020) investigated the hygroscopic behavior of 100-nm D-glucose aerosol particles using a HHTDMA in deliquescence, efflorescence, and restructuring modes of operation, respectively. A clear morphology effect on the hygroscopicity of D-glucose aerosol particles is observed in the RH range from 2 % to 96 % RH. No prompt phase transitions are observed during in both deliquescence and efflorescence measurement modes. Estillore et al. (2017) observed a slightly amorphous structure of D-glucose particles under ambient conditions using an atomic force microscopy and D-glucose particles grow through gradual water uptake where the solid-liquid phase transition is non-discrete. Thus, a continuous growth/shrink of diameter in both deliquescence and efflorescence modes is explained by the lack of crystallization of D-glucose nanoparticles upon drying to low RH below 10%.

设置了格式: 字体颜色: 文字 1

Figure 8a shows the size dependence of measured hygroscopic growth factors of D-glucose nanoparticles in the size range from 6 to 100 nm, with differences in growth factor up to 0.14 between 100-nm and 6-nm nanoparticles at 90 % RH (Fig. S2). A weak size dependence on the hygroscopic growth factors of D-glucose nanoparticles is observed in the size range from 20 to 100 nm, which is similar to observation for levoglucosan nanoparticles with diameters down to 20 nm. However, there is a strong size-dependent growth factor of D-glucose nanoparticles with diameters from 6 to 20 nm, especially at high RH, i.e., $RH > \sim 80\%$. There is no evident difference in hygroscopic growth factors of D-glucose nanoparticles at RH below 80 % in size range from 6 to 100 nm. The reason that the growth factor shows size dependence only in the regime of hygroscopic growth ($RH > 80\%$), and not in the regime of water adsorption ($RH < 80\%$) has not been explained before. Our hypothesis is that the distinct behaviors between high RH and low RH region can be attributed to the distinct size effect on the hygroscopic growth and adsorption, i.e., the growth factor shows size dependence only in the regime of hygroscopic growth ($RH > 80\%$), and not in the regime of water adsorption ($RH < 80\%$). Figure 8b further shows the clear change in the

设置了格式: 字体颜色: 文字 1

hygroscopic growth factor of D-glucose aerosol nanoparticles with diameters from 100 down to 6 nm at 87 % RH.

The hygroscopic growth factor of D-glucose nanoparticles is almost unchanged with diameters from 20 to 100 nm. However, a markedly increase in the hygroscopic growth factor of D-glucose aerosol nanoparticles is observed as size increases from 6 to 20 nm. E-AIM model predict well the measured hygroscopic growth factors of D-glucose with diameters smaller than 15 nm at 87 % RH, while ideal solution theory agrees with hygroscopic measurement results of D-glucose with diameters higher than 60 nm at the same RH. The use of DKA methods leads to a good agreement between measurements and model predictions.

The measured hygroscopic growth factors of D-glucose nanoparticles with diameters of 6 and 100 nm are compared with the model and theory shown in Fig. 9, Fig. S3, and Fig. S4, respectively.

Ideal solution theory is applied to predict the hygroscopic growth factor of organics in the ideal solution. Figure 9a and Fig. S3 show that the measured growth factors of 100-nm D-glucose nanoparticles are lower than predicted growth factors from E-AIM (standard UNIFAC) model, especially at RH below 85 %. Also, E-AIM (standard UNIFAC) model could predict well the measured hygroscopic growth factor of 6-nm D-glucose aerosol nanoparticles at RH above 40 % shown in Fig. 9a and Fig. S3. The possible reason for discrepancies between E-AIM (standard UNIFAC) model and measurements is inaccurate thermodynamic parameters (e.g., water activity, surface tension) estimated by the E-AIM (standard UNIFAC) model without consideration intramolecular interaction (Fredenslund et al., 1975; Hansen et al., 1991; Fredenslund and Sørensen,

1994; Mochida and Kawamura, 2004). D-glucose contains five OH groups in series, hydrogen bond could potentially exist and affects the E-AIM (standard UNIFAC) model-measurement agreement for D-glucose aerosol nanoparticles system (Mochida and Kawamura, 2004; Lei et al., 2014, 2018). Using ideal solution theory is to predict the hygroscopic curve of D-glucose nanoparticles with diameters of 6-100 nm shown in Fig. 9b and Fig. S3. There is a good agreement

删除了: To have a clear observation for size dependence of the hygroscopic growth factor of D-glucose aerosol nanoparticles with diameters down to 6 nm, Fig. 8b shows the change in the hygroscopic growth factor of D-glucose aerosol nanoparticles with diameters from 100 down to 6 nm at 87 % RH.

删除了: Note that, E-AIM (standard UNIFAC) model prediction is optimized for organic compounds with lesser polar groups in series, i.e., intramolecular interaction, such as hydrogen bond between polar groups, may result in model prediction inaccuracy.

设置了格式: 字体颜色: 文字 1

设置了格式: 字体颜色: 文字 1

520 between measured growth factors of 100-nm D-glucose and ideal theory predictions. This suggests
521 that thermodynamic parameters (e.g., water activity, surface tension, and solution density) assumed
522 by the ideal solution theory are accurate to use in Eq. (1) and (2) for predicting the hygroscopic
523 curve of D-glucose nanoparticles with large sizes (e.g., 60, 100 nm). However, an underestimation
524 of growth factors of 6-nm D-glucose nanoparticles has been shown in Fig. 9b and Fig. S3 by ideal
525 solution theory prediction at RH above 30 %. The possible reason is the unfavorable assumption
526 of ideal solution theory. As D-glucose size decreases from 20 to 6 nm, D-glucose nanodroplets
527 could be highly supersaturated in concentration compared to the dilution solution. However, the
528 current thermodynamic models (e.g., E-AIM) mostly rely on the concentration-dependent
529 thermodynamic properties (such as water activity) derived from the measurements of large aerosol
530 particles or even bulk samples (Tang and Munkelwitz, 1994; Tang, 1996; Pruppacher and Klett,
531 1997; Clegg et al., 1998). They are thus difficult or impossible to apply to describe the hygroscopic
532 behavior of sub-10 nm nanoparticles, which can often be supersaturated in concentration compared
533 to bulk solutions (Cheng et al., 2015; Wang et al., 2018). Thus, nanosize effect on these
534 thermodynamic properties has been taken into account the models and theories (Cheng et al., 2015).
535 Combination of DKA methods and hygroscopic measurements of aerosol nanoparticles in the
536 different sizes can use to determine the thermodynamic properties (e.g., water activity) in the highly
537 supersaturated concentration range (Cheng et al., 2015). Therefore, as shown in Fig. 9c and Fig.
538 S4, the use of the DKA method leads a good agreement with the measured hygroscopic growth
539 factors of Glucose nanoparticles with diameters from 100 down to 6 nm.

540

541 4 Conclusions

删除了: ve

删除了: in

544 In this study, we investigate the hygroscopic behavior of levoglucosan and D-glucose nanoparticles
545 with diameters down to 6 nm using a nano-HTDMA. Due to the larger impact of evaporation of
546 sub-20 nm levoglucosan nanoparticles in the nano-HTDMA system, we measure hygroscopic
547 growth factor of levoglucosan with diameters down to 20 nm. There is a weak size dependence of
548 hygroscopic growth factor of levoglucosan and D-glucose with diameters down to 20 nm, while a
549 strong size dependence of the hygroscopic growth factor of D-glucose has been clearly observed
550 in the size range from 6 to 20 nm. No prompt phase transitions occur in both deliquescence and
551 efflorescence modes for both levoglucosan and D-glucose nanoparticles. By comparing with the
552 KD-derived water activity, Köhler, E-AIM model, and DKA-derived data, the predicted water
553 activity of aqueous organic solution (levoglucosan and D-glucose) is consistent with observation
554 data from references in the low solute concentration ($< 20 \text{ mol kg}^{-1}$) but failed in the solute
555 concentration ($> 20 \text{ mol kg}^{-1}$). In addition, ideal solution theory predicts well the hygroscopic
556 behavior of two specific organics with diameters higher than 60 nm (levoglucosan and D-glucose),
557 while hygroscopic growth factor of D-glucose down to 6 nm in size is in good agreement with E-
558 AIM (standard UNIFAC) model prediction at high RH. The use of the DKA method leads to a
559 good agreement with measured hygroscopic growth factor of glucose nanoparticles with diameters
560 from 100 down to 6 nm.

561

562 **Data availability**

563 Reader who are interested in the data should contact Yafang Cheng (Yafang.cheng@mpic.de).

564 **Competing interests**

删除了: Biomass burning is an important source of anthropogenic atmospheric aerosols. Aerosol particles in the biomass burning smoke enriched with hygroscopic behavior are suggested to act as efficient CCN. It is well known that aerosol population can appear as externally mixed or internally mixed (homogeneously internally, core-shell internally) in the biomass burning processes. The mixing structure has an important effect on the hygroscopic behavior of aerosol particles, especially for sub-100 nm size range. We will be able to investigate the effect of the mixing state on the hygroscopic behavior of aerosol nanoparticles from biomass burning in different sizes. This will further help us to understand their interaction with water vapor.

Some authors are members of the editorial board of journal Atmospheric Chemistry Physics. The peer-review process was guided by an independent editor, and the authors have also no other competing interests to declare.

删除了:

Acknowledgement

删除了:

This study was supported by the Max Planck Society (MPG) and Leibniz Society. T.L acknowledges the support from China Scholarship Council (CSC). Y. C. would like to acknowledge the Minerva Program of MPG.

Author contributions: Y.C. and H.S. designed and led the study. T.L. performed the experiments. All co-authors discussed the results and commented on the manuscript. T.L. wrote the manuscript with input from all co-authors.

删除了:

4 References

Andreae, M. O. and Gelencsér, A.: Black carbon or brown carbon? The nature of light-absorbing carbonaceous aerosols, Atmos. Chem. Phys., 6, 3131–3148, <https://doi.org/10.5194/acp-6-3131-2006>, 2006.

Bhandari, B. and Bareyre, I.: Estimation of crystalline phase present in the glucose crystal–solution mixture by water activity measurement, LWT - Food Science and Technology, 36, 729-733, 2003.

Bhattarai, H., Saikawa, E., Wan, X., Zhu, H., Ram, K., Gao, S., Kang, S., Zhang, Q., Zhang, Y., Wu, G., Wang, X., Kawamura, K., Fu, P., and Cong, Z.: Levoglucosan as a tracer of biomass burning: Recent progress and perspectives, Atmos. Res., 220, 20–33, 2019.

Biskos, G., Malinowski, A., Russell, L. M., Buseck, P. R., and Martin, S. T.: Nanosize effect on the deliquescence and the efflorescence of sodium chloride particles, Aerosol Sci. Technol., 40, 97-106, 2006a.

设置了格式: 字体颜色: 自动设置

604 Biskos, G., Paulsen, D., Russell, L. M., Buseck, P. R., and Martin, S. T.: Prompt deliquescence and
605 efflorescence of aerosol nanoparticles, *Atmos. Chem. Phys.*, 6, 4633–4642,
606 <https://doi.org/10.5194/acp-6-4633-2006>, 2006b.

607 Biskos, G., Russell, L. M., Buseck, P. R., and Martin, S. T.: Nanosize effect on the hygroscopic
608 growth factor of aerosol particles, *Geophys. Res. Lett.*, 33, L07801,
609 [doi:10.1029/2005GL025199](https://doi.org/10.1029/2005GL025199), 2007.

610 Bohren, C. and Huffman, D.: Absorption and scattering of light by small particles, Wiley-VCH,
611 New York, USA, 2004.

612 Bzdek, B. R., Zordan, C. A., Luther, G. W., and Johnston, M. V.: Nanoparticle Chemical
613 Composition During New Particle Formation, *Aerosol Science and Technology*, 45, 1041-
614 1048, 2011.

615 Chan, M. N., Choi, M. Y., Ng, N. L., and Chan, C. K.: Hygroscopicity of water-soluble organic
616 compounds in atmospheric aerosols: Amino acids and biomass burning derived organic species,
617 *Environ. Sci. Technol.*, 39, 1555-1562, 2005.

618 Chan, M. N. ~~and, Chan, C.~~ K.: Mass transfer effects in hygroscopic measurements of aerosol
619 particles, *Atmos. Chem. Phys.*, 5, 2703–2712, <https://doi.org/10.5194/acp-5-2703-2005>, 2005.

620 Charlson, R. J., Schwartz, S. E., Hales, J. M., Cess, R. D., Coakley, J. A., Hansen, J. E., and
621 Hoffmann, D. J.: Climate forcing by anthropogenic aerosols, *Science*, 255, 423-430, 1992.

622 Chen, Da-Ren, David Y.H. Pui, and Stanley L. Kaufman.: Electro spraying of conducting liquids
623 for monodisperse aerosol generation in the 4 nm to 1.8 nm diameter range, *J. Aerosol Sci.*,
624 26:963-977.

625 Cheng, Y. F., Su, H., Koop, T., Mikhailov, E., and Pöschl, U.: Size dependence of phase transitions
626 in aerosol nanoparticles, *Nat. Commun.*, 6, 5923, [doi:10.1038/ncomms6923](https://doi.org/10.1038/ncomms6923), 2015.

删除了:C

删除了:a.

设置了格式: 字体颜色: 自动设置

629 Cheng, Y. F., Su, H., Rose, D., Gunthe, S. S., Berghof, M., Wehner, B., Achtert, P., Nowak, A.,
630 Takegawa, N., Kondo, Y., Shiraiwa, M., Gong, Y. G., Shao, M., Hu, M., Zhu, T., Zhang, Y.
631 H., Carmichael, G. R., Wiedensohler, A., Andreae, M. O., and Pöschl, U.: Size-resolved
632 measurement of the mixing state of soot in the megacity Beijing, China: diurnal cycle, aging
633 and parameterization, *Atmos. Chem. Phys.*, 12, 4477–4491, [https://doi.org/10.5194/acp-12-](https://doi.org/10.5194/acp-12-4477-2012)
634 4477-2012, 2012.

635 Chýlek, P. and Coakley, J. A.: Aerosols and climate, *Science*, 183, 75-77, 1974.

636 Clegg, S. L., Brimblecombe, P., and Wexler, A. S.: Thermodynamic model of the system
637 $\text{H}^+ - \text{NH}_4^+ - \text{SO}_4^{2-} - \text{NO}_3^- - \text{H}_2\text{O}$ at tropospheric temperatures, *J. Phys. Chem. A*, 102, 2137–2154,
638 doi:10.1021/Jp973042r, 1998.

639 Clegg, S. L., Seinfeld, J. H., and Brimblecombe, P.: Thermodynamic modelling of aqueous
640 aerosols containing electrolytes and dissolved organic compounds, *J. Aerosol Sci.*, 32, 713–
641 738, doi:10.1016/s0021-8502(00)00105-1, 2001.

642 Clegg, S. L. and Seinfeld, J. H.: Thermodynamic models of aqueous solutions containing in-
643 organic electrolytes and dicarboxylic acids at 298.15 K. 2. Systems including dissociation
644 equilibria, *J. Phys. Chem. A*, 110, 5718–5734, doi:10.1021/jp056150j, 2006.

645 Comesaña, J. F., Correa, A., and Sereno, A. M.: Water activity at 35 °C in ‘sugar’ + water and
646 ‘sugar’ + sodium chloride + water systems, *Int. J. Food Sci. Tech.*, 36, 655-661, 2001.

647 Dick, W. D., Saxena, P., and McMurry, P. H.: Estimation of water uptake by organic compounds
648 in submicron aerosols measured during the Southeastern Aerosol and Visibility Study, *J. Geo-*
649 *phys. Res.-Atmos.*, 105, 1471–1479, doi:10.1029/1999jd901001, 2000.

650 Dunne, E. M., Gordon, H., Kürten, A., Almeida, J., Duplissy, J., Williamson, C., Ortega, I. K.,
651 Pringle, K. J., Adamov, A., Baltensperger, U., Barmet, P., Benduhn, F., Bianchi, F.,
652 Breitenlechner, M., Clarke, A., Curtius, J., Dommen, J., Donahue, N. M., Ehrhart, S., Flagan,

带格式的: 正文, 两端对齐, 缩进: 左侧: 0 厘米, 悬挂缩进: 2 字符, 首行缩进: -2 字符, 行距: 2 倍行距

设置了格式: 字体颜色: 自动设置

设置了格式: 字体颜色: 自动设置, 下标

设置了格式: 字体颜色: 自动设置

R. C., Franchin, A., Guida, R., Hakala, J., Hansel, A., Heinritzi, M., Jokinen, T., Kangasluoma, J., Kirkby, J., Kulmala, M., Kupc, A., Lawler, M. J., Lehtipalo, K., Makhmutov, V., Mann, G., Mathot, S., Merikanto, J., Miettinen, P., Nenes, A., Onnela, A., Rap, A., Reddington, C. L. S., Riccobono, F., Richards, N. A. D., Rissanen, M. P., Rondo, L., Sarnela, N., Schobesberger, S., Sengupta, K., Simon, M., Sipilä, M., Smith, J. N., Stozkhov, Y., Tomé, A., Tröstl, J., Wagner, P. E., Wimmer, D., Winkler, P. M., Worsnop, D. R., and Carslaw, K. S.: Global atmospheric particle formation from CERN CLOUD measurements, *Science.*, 354, 1119-1124, 2016.

Duplissy, J., Gysel, M., Sjogren, S., Meyer, N., Good, N., Kammermann, L., Michaud, V., Weigel,

R., Martins dos Santos, S., Gruening, C., Villani, P., Laj, P., Sellegri, K., Metzger, A., McFiggans, G. B., Wehrle, G., Richter, R., Dommen, J., Ristovski, Z., Baltensperger, U., and Weingartner, E.: Intercomparison study of six HTDMAs: results and recommendations, *Atmos. Meas. Tech.*, 2, 363–378, <https://doi.org/10.5194/amt-2-363-2009>, 2009.

Dusek, U., Frank, G. P., Curtius, J., Drewnick, F., Schneider, J., Kürten, A., Rose, D., Andreae, M. O., Borrmann, S., and Pöschl, U.: Enhanced organic mass fraction and decreased hygroscopicity of cloud condensation nuclei (CCN) during new particle formation events, *Geophys. Res. Lett.*, 37, 2010.

Dutcher, C. S., Ge, X., Wexler, A. S. & Clegg, S. L. An Isotherm-Based Thermodynamic Model of Multicomponent Aqueous Solutions, Applicable Over the Entire Concentration Range. *J. Phys. Chem. A* 117, 3198-3213 (2013).

Elias, V. O., Simoneit, B. R. T., Cordeiro, R. C., and Turcq, B.: Evaluating levoglucosan as an indicator of biomass burning in Carajás, amazônia: a comparison to the charcoal record22Associate editor: R. Summons, *Geochim. Cosmochim. Acta.*, 65, 267-272, 2001.

设置了格式: 字体颜色: 自动设置

676 Estillore, A. D., Morris, H. S., Or, V. W., Lee, H. D., Alves, M. R., Marciano, M. A., Laskina, O.,
677 Qin, Z., Tivanski, A. V., and Grassian, V. H.: Linking hygroscopicity and the surface
678 microstructure of model inorganic salts, simple and complex carbohydrates, and authentic sea
679 spray aerosol particles, *Phys. Chem. Chem. Phys.*, 19, 21101-21111, 2017.

680 Ferreira, O., Brignole, E. A., and Macedo, E. A.: Phase equilibria in sugar solutions using the A-
681 UNIFAC model, *Ind. Eng. Chem. Res.*, 42 (24), 6212–6222, 2003.

682 Fraser, M. P. and Lakshmanan, K.: Using Levoglucosan as a Molecular Marker for the Long-Range
683 Transport of Biomass Combustion Aerosols, *Environ. Sci. Technol.*, 34, 4560-4564, 2000.

684 Fredenslund, A., Jones, R. L., and Prausnitz, J. M.: Group-contribution estimation of activity-
685 coefficients in nonideal liquid-mixtures, *Aiche J.*, 21, 1086–1099, doi:10.1002/aic.690210607,
686 1975.

687 Hämeri, K., Laaksonen, A., Väkevä, M., and Suni, T.: Hygroscopic growth of ultrafine sodium
688 chloride particles, *J. Geophys. Res.*, 106, 20 749–20 757, 2001.

689 Hämeri, K., Väkevä, M., Hansson, H.-C., and Laaksonen, A.: Hygroscopic growth of ultrafine
690 ammonium sulfate aerosol measured using an ultrafine tandem differential mobility analyzer,
691 *J. Geophys. Res.*, 105, 22 231–22 242, 2000.

692 Hansen, H. K., Rasmussen, P., Fredenslund, A., Schiller, M., and Gmehling, J.: Vapor–liquid
693 equilibria by UNIFAC group contribution. 5. Revision and extension, *Ind. Eng. Chem. Res.*,
694 30, 2352–2355, doi:10.1021/ie00058a017, 1991.

695 Hennigan, Christopher J.; Sullivan, Amy P.; Collett, Jeffrey L.; Robinson, Allen L., Levoglucosan
696 stability in biomass burning particles exposed to hydroxyl radicals. *Geophysical Research*
697 *Letters*, 37(9), doi:10.1029/2010gl043088, 2010.

698 Kerminen, V.-M.: The effects of particle chemical character and atmospheric processes on particle
699 hygroscopic properties, *J. Aerosol Sci.*, 28, 121–132, 1997.

设置了格式: 字体颜色: 自动设置

删除了:

701 Keskinen, H., Virtanen, A., Joutsensaari, J., Tsagkogeorgas, G., Duplissy, J., Schobesberger, S.,
 702 Gysel, M., Riccobono, F., Slowik, J. G., Bianchi, F., Yli-Juuti, T., Lehtipalo, K., Rondo, L.,
 703 Breitenlechner, M., Kupc, A., Almeida, J., Amorim, A., Dunne, E. M., Downard, A. J.,
 704 Ehrhart, S., Franchin, A., Kajos, M. K., Kirkby, J., Kürten, A., Nieminen, T., Makhmutov, V.,
 705 Mathot, S., Miettinen, P., Onnela, A., Petäjä, T., Praplan, A., Santos, F. D., Schallhart, S.,
 706 Sipilä, M., Stozhkov, Y., Tomé, A., Vaattovaara, P., Wimmer, D., Prevot, A., Dommen, J.,
 707 Donahue, N. M., Flagan, R. C., Weingartner, E., Viisanen, Y., Riipinen, I., Hansel, A., Curtius,
 708 J., Kulmala, M., Worsnop, D. R., Baltensperger, U., Wex, H., Stratmann, F., and Laaksonen,
 709 A.: Evolution of particle composition in CLOUD nucleation experiments, *Atmos. Chem.*
 710 *Phys.*, 13, 5587–5600, <https://doi.org/10.5194/acp-13-5587-2013>, 2013.

711 Kim, J., Ahlm, L., Yli-Juuti, T., Lawler, M., Keskinen, H., Tröstl, J., Schobesberger, S., Duplissy,
 712 J., Amorim, A., Bianchi, F., Donahue, N. M., Flagan, R. C., Hakala, J., Heinritzi, M., Jokinen,
 713 T., Kürten, A., Laaksonen, A., Lehtipalo, K., Miettinen, P., Petäjä, T., Rissanen, M. P., Rondo,
 714 L., Sengupta, K., Simon, M., Tomé, A., Williamson, C., Wimmer, D., Winkler, P. M., Ehrhart,
 715 S., Ye, P., Kirkby, J., Curtius, J., Baltensperger, U., Kulmala, M., Lehtinen, K. E. J., Smith, J.
 716 N., Riipinen, I., and Virtanen, A.: Hygroscopicity of nanoparticles produced from
 717 homogeneous nucleation in the CLOUD experiments, *Atmos. Chem. Phys.*, 16, 293–304,
 718 <https://doi.org/10.5194/acp-16-293-2016>, 2016.

719 Koehler, K. A., Kreidenweis, S. M., DeMott, P. J., Prenni, A. J., Carrico, C. M., Ervens, B., and
 720 Feingold, G.: Water activity and activation diameters from hygroscopicity data - Part II:
 721 Application to organic species, *Atmos. Chem. Phys.*, 6, 795-809, 2006.

722 Köhler, H.: The nucleus in and the growth of hygroscopic droplets, *Trans. Faraday Soc.*, 32, 1152–
 723 1161, 1936.

724 Kreidenweis, S. M., Koehler, K., DeMott, P. J., Prenni, A. J., Carrico, C., and Ervens, B.: Water
725 activity and activation diameters from hygroscopicity data - Part I: Theory and application to
726 inorganic salts, *Atmos. Chem. Phys.*, 5, 1357–1370, <https://doi.org/10.5194/acp-5-1357-2005>,
727 2005.

728 Kulmala, M., Kontkanen, J., Junninen, H., Lehtipalo, K., Manninen, H. E., Nieminen, T., Petäjä,
729 T., Sipilä, M., Schobesberger, S., Rantala, P., Franchin, A., Jokinen, T., Järvinen, E., Äijälä,
730 M., Kangasluoma, J., Hakala, J., Aalto, P. P., Paasonen, P., Mikkilä, J., Vanhanen, J., Aalto,
731 J., Hakola, H., Makkonen, U., Ruuskanen, T., Mauldin, R. L., Duplissy, J., Vehkamäki, H.,
732 Bäck, J., Kortelainen, A., Riipinen, I., Kurtén, T., Johnston, M. V., Smith, J. N., Ehn, M.,
733 Mentel, T. F., Lehtinen, K. E. J., Laaksonen, A., Kerminen, V.-M., and Worsnop, D. R.: Direct
734 Observations of Atmospheric Aerosol Nucleation, *Science*, 339, 943-946, 2013.

735 Lei, T., Ma, N., Hong, J., Tuch, T., Wang, X., Wang, Z., Pöhlker, M., Ge, M., Wang, W., Mikhailov,
736 E., Hoffmann, T., Pöschl, U., Su, H., Wiedensohler, A., and Cheng, Y.: Nano-hygroscopicity
737 tandem differential mobility analyzer (nano-HTDMA) for investigating hygroscopic
738 properties of sub-10 nm aerosol nanoparticles, *Atmos. Meas. Tech.*, 13, 5551–5567,
739 <https://doi.org/10.5194/amt-13-5551-2020>, 2020

740 Lei, T., Zuend, A., Cheng, Y., Su, H., Wang, W., and Ge, M.: Hygroscopicity of organic surrogate
741 compounds from biomass burning and their effect on the efflorescence of ammonium
742 sulfate in mixed aerosol particles, *Atmos. Chem. Phys.*, 18, 1045-1064, 2018.

743 Lei, T., Zuend, A., Wang, W. G., Zhang, Y. H., and Ge, M. F.: Hygroscopicity of organic
744 compounds from biomass burning and their influence on the water uptake of mixed organic
745 ammonium sulfate aerosols, *Atmos. Chem. Phys.*, 14, 11165-11183, 2014.

746 Lihavainen, H., Kerminen, V.-M., Komppula, M., Hatakka, J., Aaltonen, V., Kulmala, M., and
747 Viisanen, Y.: Production of “potential” cloud condensation nuclei associated with

atmospheric new-particle formation in northern Finland, J. Geophys. Res., 108, 4782,
doi:10.1029/2003JD003887, 2003.

Mikhailov, E., Vlasenko, S., Martin, S. T., Koop, T., and Pöschl, U.: Amorphous and crystalline
aerosol particles interacting with water vapor: conceptual framework and experimental
evidence for restructuring, phase transitions and kinetic limitations, Atmos. Chem. Phys., 9,
9491–9522, <https://doi.org/10.5194/acp-9-9491-2009>, 2009.

Mikhailov, E. F. and Vlasenko, S. S.: High humidity tandem differential mobility analyzer for
accurate determination of aerosol hygroscopic growth, microstructure and activity
coefficients over a wide range of relative humidity, Atmos. Meas. Tech., 13, 2035–2056,
<https://doi.org/10.5194/amt-13-2035-2020>, 2020.

Mikhailov, E. F., Vlasenko, S. S., and Ryshkevich, T. I.: Influence of chemical composition and
microstructure on the hygroscopic growth of pyrogenic aerosol, Izv. Atmos. Ocean. Phy., 44,
416–431, 2008.

Mochida, M. and Kawamura, K.: Hygroscopic properties of levoglucosan and related organic
compounds characteristic to biomass burning aerosol particles, J. Geophys. Res.-Atmos., 109,
D21202, doi:10.1029/2004jd004962, 2004.

Peng, C., Chow, A. H. L., and Chan, C. K.: Hygroscopic study of glucose, citric acid, and sorbitol
using an electrodynamic balance: comparison with UNIFAC Predictions, Aerosol Sci.
Technol., 35 (3), 753–758, 2001.

Pruppacher, H. R. and Klett, J. D: Microphysics of clouds and precipitation, Kluwer Academic
Publishers, 1997.

Pöhlker, M. L., Pöhlker, C., Ditas, F., Klimach, T., Hrabě de Angelis, I., Araújo, A., Brito, J.,
Carbone, S., Cheng, Y., Chi, X., Ditz, 105 R., Gunthe, S. S., Kesselmeier, J., Könnemann, T.,
Lavrič, J. V., Martin, S. T., Mikhailov, E., Moran-Zuloaga, D., Rose, D., Saturno, J., Su, H.,

设置了格式: 字体颜色: 自动设置

设置了格式: 字体颜色: 自动设置

Thalman, R., Walter, D., Wang, J., Wolff, S., Barbosa, H. M. J., Artaxo, P., Andreae, M. O.,
and Pöschl, U.: Longterm observations of cloud condensation nuclei in the Amazon 110 rain
forest – Part 1: Aerosol size distribution, hygroscopicity, and new model parametrizations for
CCN prediction, *Atmos. Chem. Phys.*, 16, 15709–15740, [https://doi.org/10.5194/acp-16-](https://doi.org/10.5194/acp-16-15709-2016)
15709-2016, 2016

Raoux, S., Rettner, C. T., Jordan-Sweet, J. L., Kellock, A. J., Topuria, T., Rice, P. M., and Miller,
D. C.: Direct observation of amorphous to crystalline phase transitions in nanoparticle arrays
of phase change materials, *J. Appl. Phys.*, 102, 094305 (2007).

Randles, C. A., Russell, L. M., and Ramaswamy, V.: Hygroscopic and optical properties of organic
sea salt aerosol and consequences for climate forcing, *Geophys. Res. Lett.*, 31, L16 108,
doi:10.1029/2004GL020628, 2004.

Seinfeld, J. H., and Pandis, S. N.: *Atmospheric Chemistry and Physics: From Air Pollution to
Climate Change* (Second edition), Wiley Interscience, New York, 2006.

Sihto, S. L., Mikkilä, J., Vanhanen, J., Ehn, M., Liao, L., Lehtipalo, K., Aalto, P. P., Duplissy, J.,
Petäjä, T., Kerminen, V. M., Boy, M., and Kulmala, M.: Seasonal variation of CCN
concentrations and aerosol activation properties in boreal forest, *Atmos. Chem. Phys.*, 11,
13269-13285, <https://doi.org/10.5194/acp-11-13269-2011>, 2011.

Simoneit, B. R. T., Schauer, J. J., Nolte, C. G., Oros, D. R., Elias, V. O., Fraser, M. P., Rogge, W.
F., and Cass, G. R.: Levoglucosan, a tracer for cellulose in biomass burning and atmospheric
particles, *Atmos. Environ.*, 33, 173-182, 1999.

Suda, S. R. and Petters, M. D.: Accurate determination of aerosol activity coefficients at relative
humidities up to 99 % using the hygroscopicity tandem differential mobility analyzer
technique, *Aerosol Sci. Technol.*, 47, 991–
1000, <https://doi.org/10.1080/02786826.2013.807906>, 2013.

删除了:

设置了格式: 字体颜色: 自动设置

设置了格式: 英语(美国)

设置了格式: 字体: (默认) Times New Roman, (中文) Times New Roman, 小四

设置了格式: 英语(美国)

带格式的: 正文, 两端对齐, 缩进: 左侧: 0 厘米, 悬挂缩进: 2 字符, 首行缩进: -2 字符

设置了格式: 字体: (默认) Times New Roman, (中文) Times New Roman, 小四

797 Su, H., Rose, D., Cheng, Y. F., Gunthe, S. S., Massling, A., Stock, M., Wiedensohler, A., Andreae,
798 M. O., and Pöschl, U.: Hygroscopicity distribution concept for measurement data analysis and
799 modeling of aerosol particle mixing state with regard to hygroscopic growth and CCN
800 activation, *Atmos. Chem. Phys.*, 10, 7489–7503, <https://doi.org/10.5194/acp-10-7489-2010>,
801 2010.

802 Svenningsson, B., Rissler, J., Swietlicki, E., Mircea, M., Bilde, M., Facchini, M. C., Decesari, S.,
803 Fuzzi, S., Zhou, J., Mønster, J., and Rosenørn, T.: Hygroscopic growth and critical
804 supersaturations for mixed aerosol particles of inorganic and organic compounds of
805 atmospheric relevance, *Atmos. Chem. Phys.*, 6, 1937–1952, 2006.

806 Tang, I. N.: Chemical and size effects of hygroscopic aerosols on light scattering coefficients, *J.*
807 *Geophys. Res.*, 101, 19 245– 19 250, 1996.

808 Tang, I. N., Fung, K. H., Imre, D. G., and Munkelwitz, H. R.: Phase Transformation and
809 Metastability of Hygroscopic Microparticles, *J. Geophys. Res.-Atmos*, 99, 18801– 18808,
810 1994.

811 Wang, J., Shilling, J. E., Liu, J., Zelenyuk, A., Bell, D. M., Petters, M. D., Thalman, R., Mei, F.,
812 Zaveri, R. A., and Zheng, G.: Cloud droplet activation of secondary organic aerosol is mainly
813 controlled by molecular weight, not water solubility, *Atmos. Chem. Phys.*, 19, 941–954, 2019.

814 Wang, Z., Cheng, Y., Ma, N., Mikhailov, E., Pöschl, U., and Su, H.: Dependence of the
815 hygroscopicity parameter κ on particle size, humidity and solute concentration: implications
816 for laboratory experiments, field measurements and model studies, *Atmos. Chem. Phys.*
817 *Discuss.*, 2017, 1–33, 2017.

818 Wang, Z., Su, H., Wang, X., Ma, N., Wiedensohler, A., Pöschl, U., and Cheng, Y.: Scanning
819 supersaturation condensation particle counter applied as a nano-CCN counter for size-

设置了格式: 字体颜色: 自动设置

设置了格式: 字体颜色: 自动设置

820 resolved analysis of the hygroscopicity and chemical composition of nanoparticles, Atmos.
821 Meas. Tech., 8, 2161–2172, <https://doi.org/10.5194/amt-8-2161-2015>, 2015.

822 Wiedensohler, A., Cheng, Y. F., Nowak, A., Wehner, B., Achtert, P., Berghof, M., Birmili, W.,
823 Wu, Z. J., Hu, M., Zhu, T., Takegawa, N., Kita, K., Kondo, Y., Lou, S. R., Hofzumahaus, A.,
824 Holland, F., Wahner, A., Gunthe, S. S., Rose, D., Su, H., and Pöschl, U.: Rapid aerosol particle
825 growth and increase of cloud condensation nucleus activity by secondary aerosol formation
826 and condensation: A case study for regional air pollution in northeastern China, J. Geophys.
827 Res.–Atmos., 114, doi:10.1029/2008JD010884, 2009.

828 Wiedensohler, A., Lütkeemeier, E., Feldpausch, M., & Helsper, C. (1986). Investigation of the
829 bipolar charge distribution at various gas conditions. J. Aerosol Sci., 17(3), 413–416.
830 [https://doi.org/10.1016/0021-8502\(86\)90118-7](https://doi.org/10.1016/0021-8502(86)90118-7).

831 Zhang, R.: Getting to the Critical Nucleus of Aerosol Formation, Science, 328, 1366-1367, 2010.

832 Zhang, R., Khalizov, A., Wang, L., Hu, M., and Xu, W.: Nucleation and Growth of Nanoparticles
833 in the Atmosphere, Chem. Re., 112, 1957-2011, 2012.

834 Zhang, R., Suh, I., Zhao, J., Zhang, D., Fortner, E. C., Tie, X., Molina, L. T., and Molina, M. J.:
835 Atmospheric New Particle Formation Enhanced by Organic Acids, Science, 304, 1487-1490,
836 2004.

837 Zamora, I., Tabazadeh, A., Golden, D., and Jacobson, M.: Hygroscopic growth of common organic
838 aerosol solutes, including humic substances, as derived from water activity measurements,
839 Journal of Geophysical Research (Atmospheres), 116, 23207, 10.1029/2011JD016067, 2011.

840 Zieger, P., Fierz-Schmidhauser, R., Weingartner, E., and Baltensperger, U.: Effects of relative
841 humidity on aerosol light scattering: results from different European sites, Atmos. Chem.
842 Phys., 13, 10609–10631, <https://doi.org/10.5194/acp-13-10609-2013>, 2013.

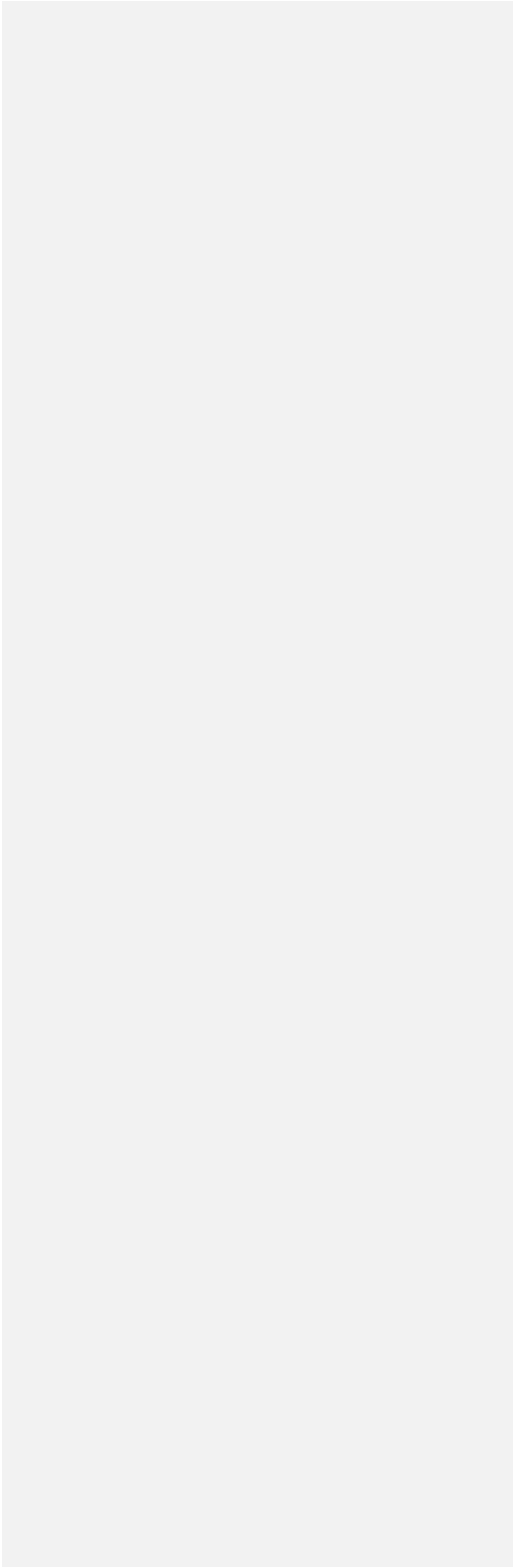
843

设置了格式: 英语(美国)

删除了:

删除了:

846
847
848
849
850
851
852
853
854
855
856
857
858
859
860
861
862
863
864
865





874

设置了格式: 字体: 10 磅

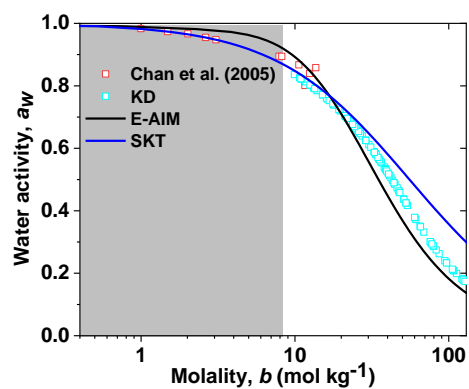


Figure 2. Concentration-dependent water activity (a_w) of levoglucosan solution. The KD-derived a_w (KD=Kreidenweis, cyan open square) is compared with observations (red open square), E-AIM (Extend-Aerosol Inorganic Model, black line), and a_w model (SKT, blue line). The light grey shaded areas mark the sub-saturated concentration with respect to bulk solution.

设置了格式: 字体颜色: 文字 1

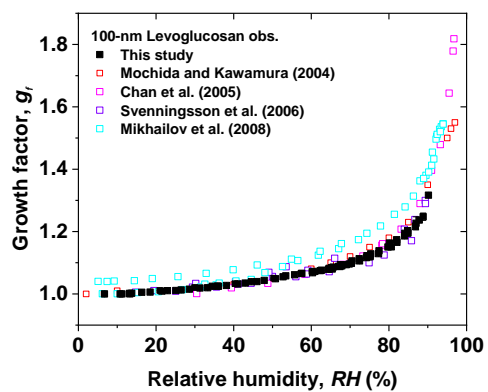


Figure 3. Hygroscopic diameter growth factor (G_f) of levoglucosan particles with dry diameter of 100 nm in both deliquescence and efflorescence mode processes (black solid square). The measured data compared with literature data from Mochida and Kawamura (2004) in both deliquescence and efflorescence modes (red open square), Chan et al. (2005) in the deliquescence mode (magenta open square), Svenningsson et al. (2006) in the deliquescence mode (violet open square), and Mikhailov et al. (2008) in both deliquescence and efflorescence modes (cyan open square).

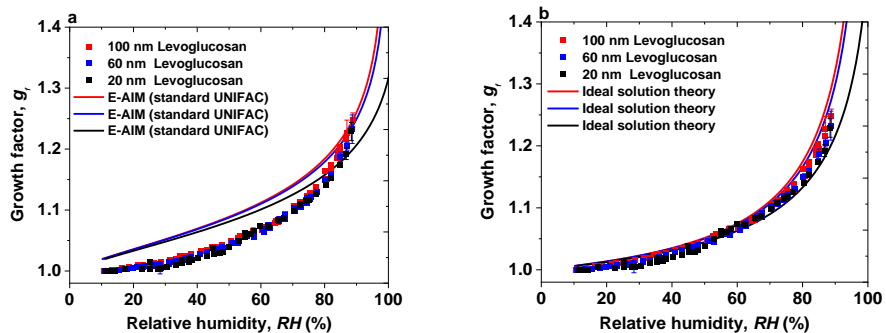


Figure 4. Hygroscopic diameter growth factor (G_p) of levoglucosan particles with dry diameter of 100 nm (red square), 60 nm (blue square), and 20 nm (green square). Köhler model curves are based on: (a) E-AIM (standard UNIFAC) (100 nm: red, 60 nm: blue, 20 nm: green line), (b) ideal solution theory (100 nm: red, 60 nm: blue, 20 nm: green line).

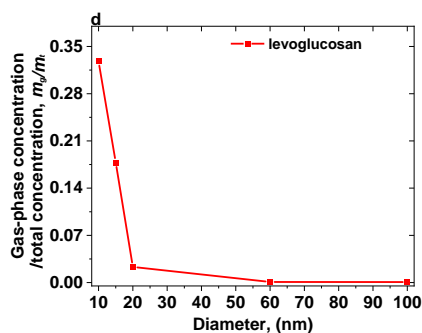
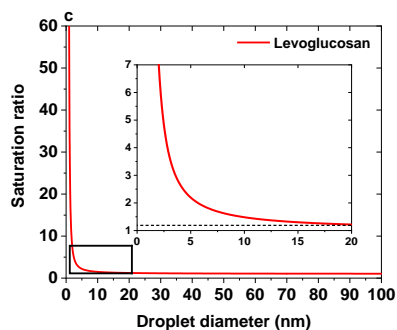
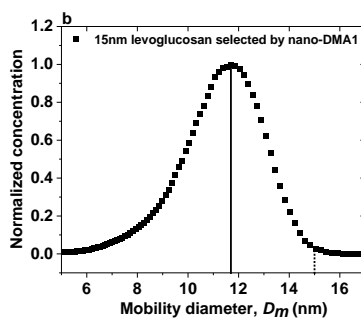
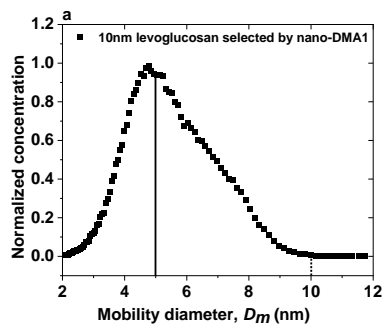


Figure 5. The normalized size distributions scanned by nano-DMA2 for: (a) 10 nm and (b) 15-nm levoglucosan at 10% at 298K. The dotted lines mark the diameters of the monodispersed nanoparticles selected by the nano-DMA1. The back solid lines mark the peak diameters from the normalized size distributions scanned by the nano-DMA2. (c) Vapor saturation ratio of levoglucosan as a function of nanodroplet diameter according to the Kelvin equation. The diameter range 0-20 nm for the saturation ratio of levoglucosan particles is shown as an inset. The value of surface tension of pure levoglucosan is 0.0227104 [J m⁻²]. (d) The ratio of gas-phase concentration (m_g) to the total concentration (m_t) of levoglucosan nanoparticles against diameter.

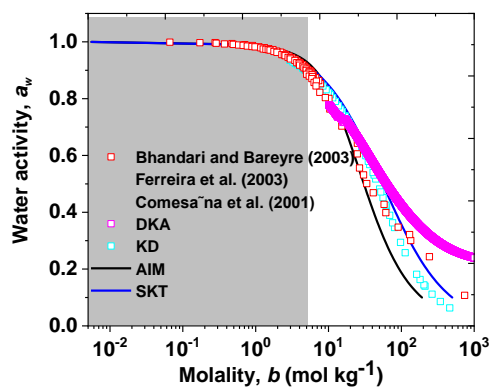


Figure 6. Concentration-dependent water activity (a_w) of D-glucose solution. The DKA-derived a_w (Differential Köhler Analysis, magenta open square) is compared with observations (red open square), E-AIM (Extend-Aerosol Inorganic Model, black line), a_w model (SKT, blue line), and parameterization model for a_w (KD=Kreidenweis, cyan open square). The light grey shaded areas mark the sub-saturated concentration with respect to bulk solution.

设置了格式: 字体颜色: 文字 1

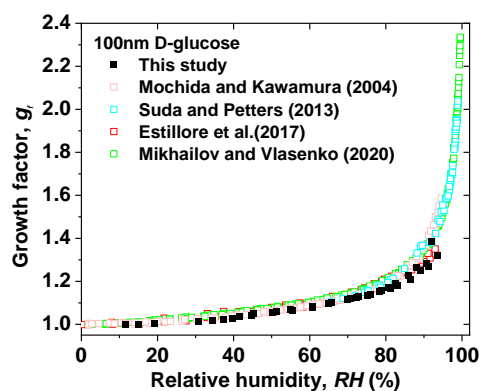


Figure 7. Hygroscopic diameter growth factor (G) of D-glucose particles with dry diameter of 100 nm in both deliquescence and efflorescence modes (black solid square). The measured data compared with reference data from Mochida and Kawamura (2004) in both deliquescence and efflorescence modes (pink open square), Suda and Petters, (20017) in deliquescence mode (violet open square), Estillore et al., (2017) in both deliquescence and efflorescence modes (red open square), and Mikhailov and Vlasenko (2020) in both deliquescence and efflorescence modes (green open square).

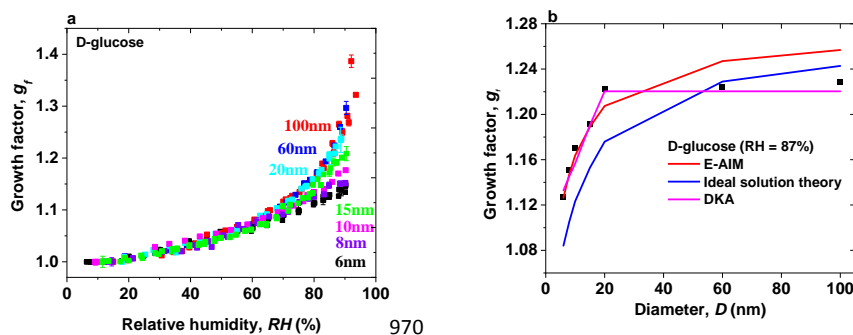


Figure 8. (a) Hygroscopic diameter growth factor (G_f) of D-glucose nanoparticles with dry diameters of 100 nm (red square), 60 nm (blue square), 20 nm (cyan square), 15 nm (green square), 10 nm (pink square), 8 nm (royal square), and 6 nm (black square). **(b)** Hygroscopic diameter growth factor (G_f , black square) of D-glucose nanoparticles with dry diameters from 6 to 100 nm at 87% RH. The measured hygroscopic growth factors of D-glucose nanoparticles with diameters from 100 down to are compared with E-AIM model (red line), ideal solution theory (blue line), and DKA prediction (pink line).

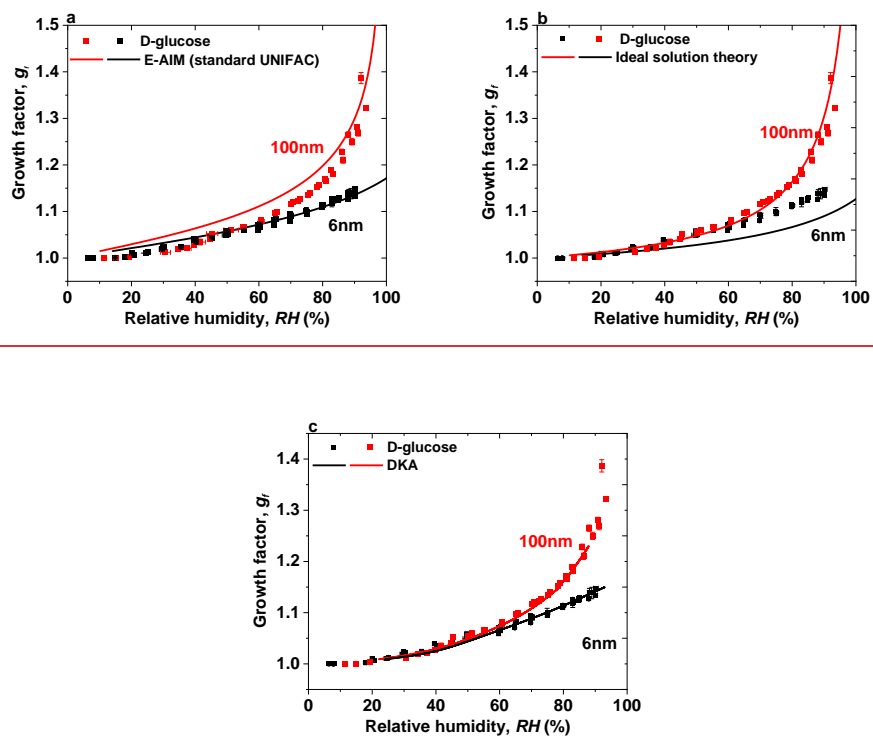


Figure 9. Hygroscopic diameter growth factor (G_r) of D-glucose nanoparticles with dry diameters of 100 nm (red square) and 6 nm (black square). Köhler model curves are based on: (a) AIM (standard UNIFAC), (100 nm: red, 6 nm: black line), (b) ideal solution theory (100 nm: red, 6 nm: black line), and (c) DKA mode (100 nm: red, 6 nm: black line).

带格式的: 缩进: 左侧: 0 厘米, 首行缩进: 0 字符

Table

Table S1. Substances and their physical properties used in this work.

Chemical compound	Chemical formula	Molar mass [gmol ⁻¹]	Density [g cm ⁻³]	Solubility mol/kg	Solution surface tension [J m ⁻²]	Manufacture
Levoglucozan	C ₆ H ₁₀ O ₅	162.141	1.69	-	0.073 ^b	Sigma-Aldrich, 99.99%
D-glucose	C ₆ H ₁₂ O ₆	180.16	1.562	5.69 ^a	0.072	Sigma-Aldrich, 99.99%

^a Ruegg and Blanc (1981)

^b Tuckermann and Cammenga (2004)

Table S2. Coefficients (a, b, c) of the fitted growth curve parameterization to measured growth factor data using Eq. (3). Measured growth factors of initial dry diameter used in Eq. (1) were firstly corrected for the Kelvin effect.

Chemical compounds	<i>a</i>	<i>b</i>	<i>c</i>
Levogluconan	0.45602	-0.69869	0.44755
D-glucose	0.30189	-0.38796	0.30478

Table S3. Equations for KD fit water activity a_w of levogluconan and D-glucose at 298K, respectively. Here x is the molality (mol kg⁻¹)

Chemical compounds	Equations
Levogluconan	$y = 1.97 * 10^{-9} * x^4 - 7.923 * 10^{-7} * x^3 + 0.0001469 * x^2 - 0.01649 * x + 0.9931$
D-glucose	$y = \frac{0.472*x^2+4.065*10^4*x+9.655}{x^3+884.4*x^2+4.063*10^4*x-0.5678}$

Table S4. Calculation of the ratio of gas-phase concentration to the total concentration for levoglucosan nanoparticles in the different sizes.

Levoglucosan diameter (nm)	The ratio of gas-phase concentration to the total concentration ^a
100	0.000811
60	0.000833097
20	0.023217028
15	0.177992638
10	0.328220471

^a See S1 section below

Figure

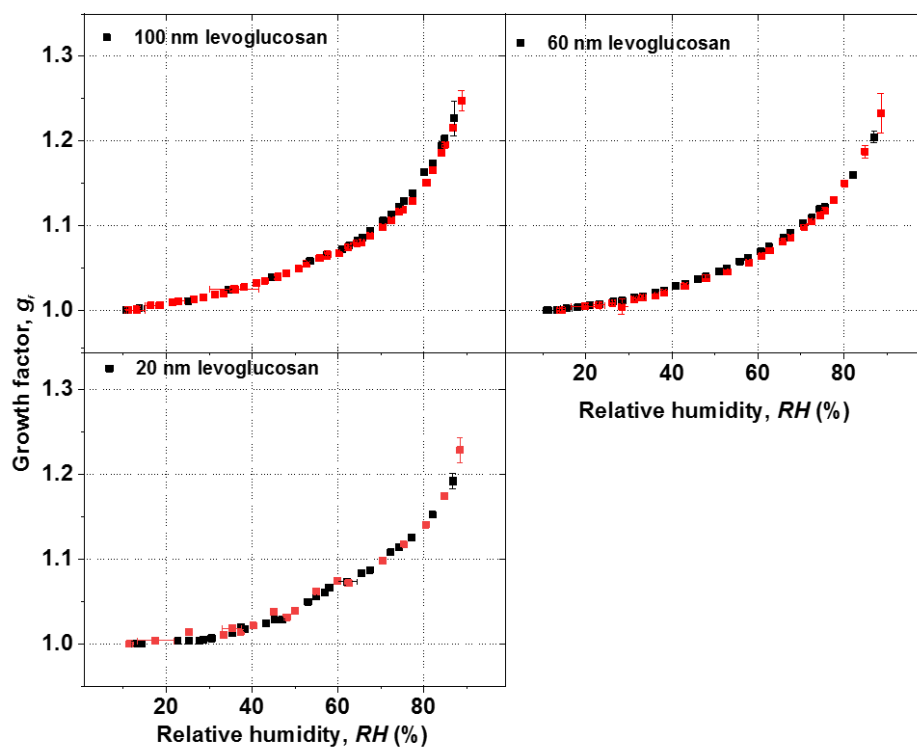


Figure S1. Mobility-diameter hygroscopic growth factors (g) of levoglucosan aerosol nanoparticles with dry mobility diameter from 20 to 100 nm in the deliquescence mode (black square and error bar) and the efflorescence mode (red square and error bar).

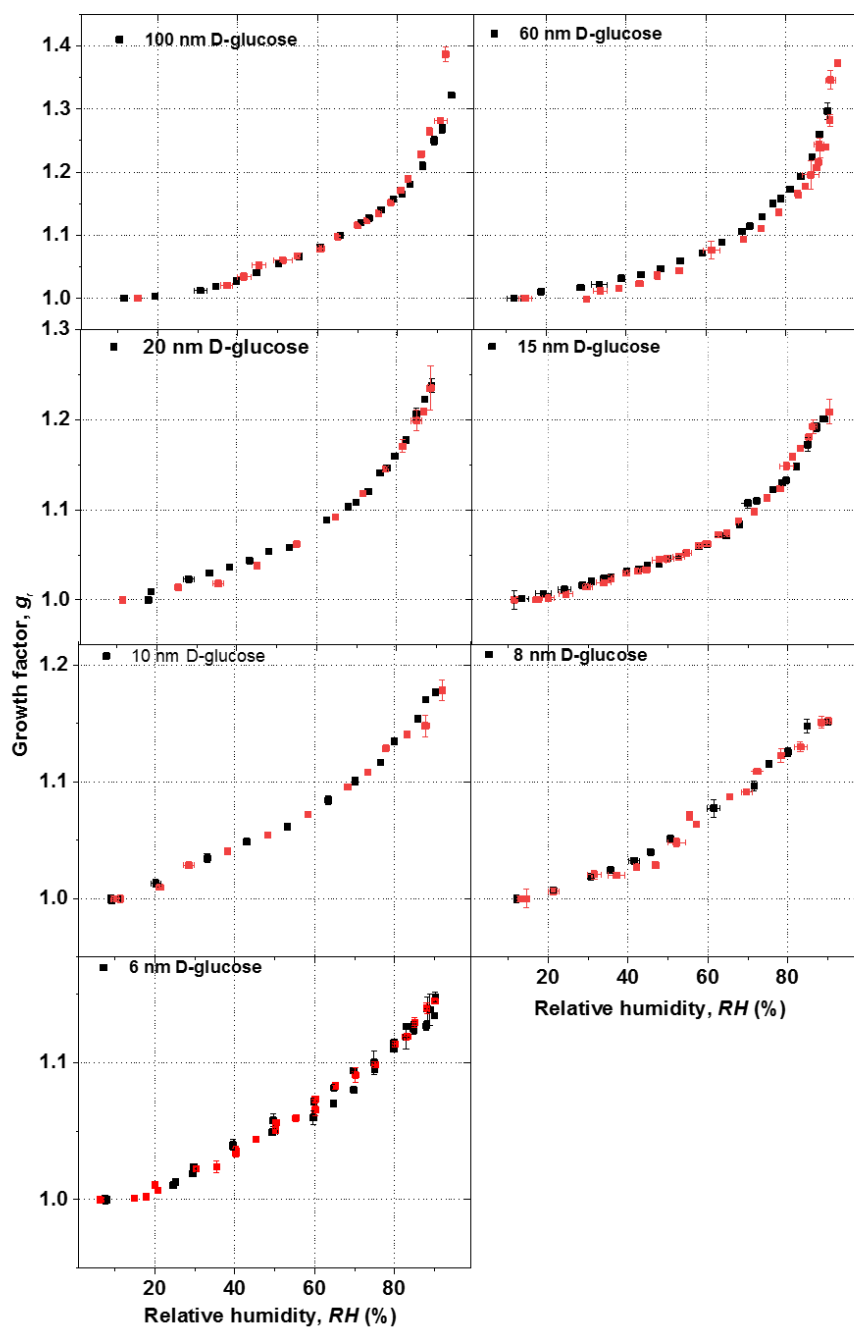


Figure S2. Mobility-diameter hygroscopic growth factors (g) of D-glucose aerosol nanoparticles with dry mobility diameter from 6 to 100 nm in the deliquescence mode (black square and error bar) and the efflorescence mode (red square and error bar).

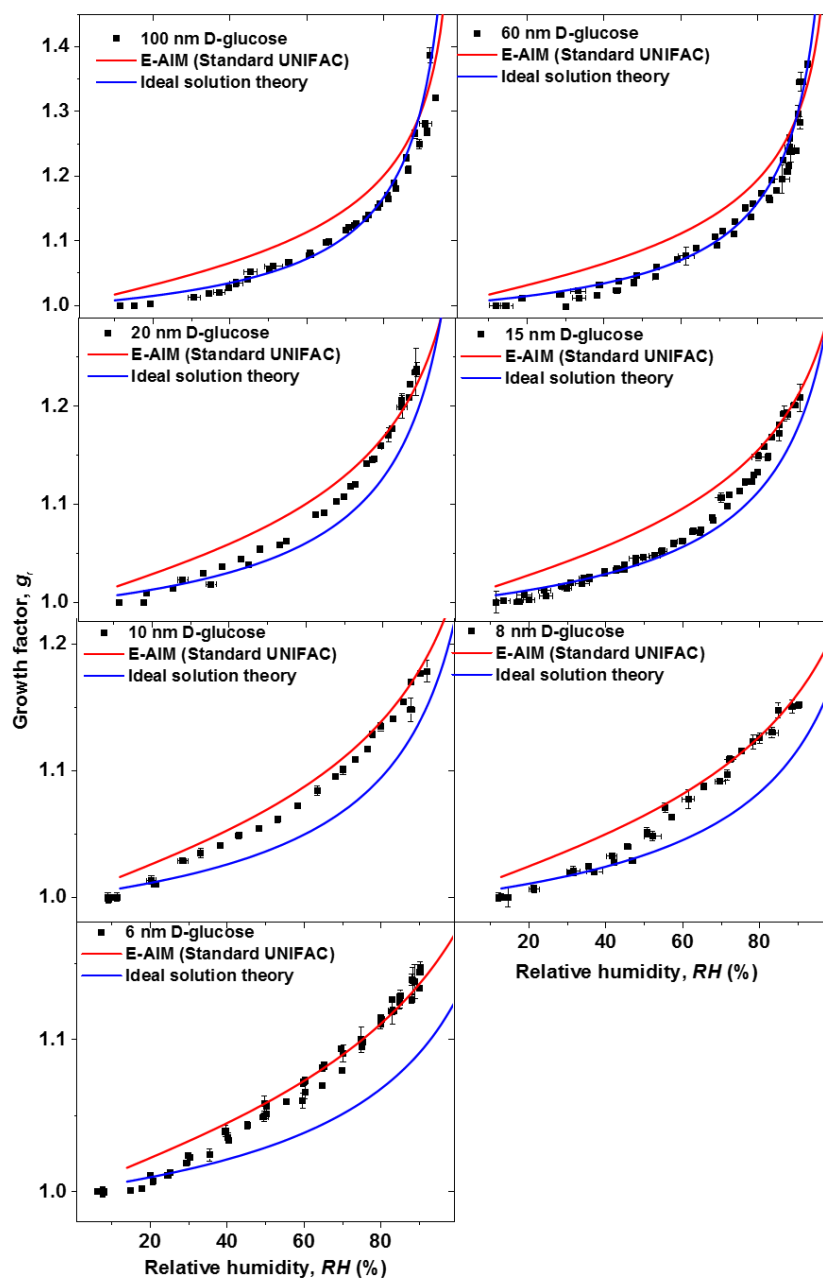


Figure S3. Mobility-diameter hygroscopic growth factors (g_r , black squares) of D-glucose aerosol nanoparticles with dry mobility diameter from 100 down to 6 nm in both deliquescence and efflorescence modes. In comparison, E-AIM (Standard UNIFAC) (red line) and Ideal solution theory (blue line) predict growth factors of D-glucose aerosol nanoparticles.

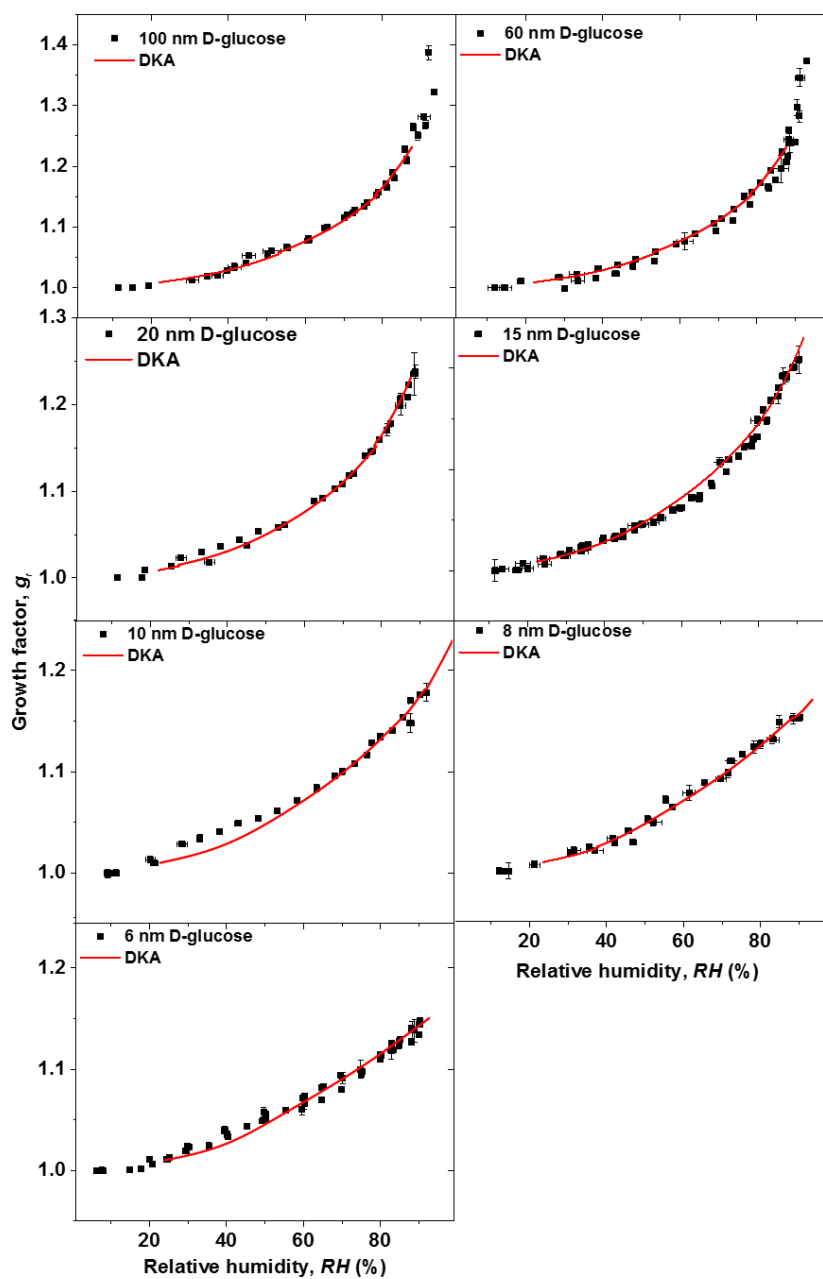


Figure S4. Mobility-diameter hygroscopic growth factors (g_f , black squares) of D-glucose aerosol nanoparticles with dry mobility diameter from 100 down to 6 nm in both deliquescence and efflorescence modes. In comparison, DKA model (red line) predicts growth factors of D-glucose aerosol nanoparticles.

S1. Calculation of ratio of gas-phase concentration to the total concentration

S1.1 Calculation of gas-phase concentration (g/cm³)

$$P_A = P_A^0 \exp\left(\frac{2\sigma M}{RT\rho_l R_p}\right) \quad (S1)$$

$$m_{gas} = \frac{PVM}{RT} \quad (S2)$$

where P_A and P_A^0 are vapor pressure, equilibrium vapor pressure, respectively. σ , M , ρ_l , and R_p mean surface tension, molecular weight of the substance, liquid-phase density, and a droplet of radius, respectively. This equation (Eq. 8) shows a relationship between mass in gas phase (m_{gas}) and pressure (P), volume (V), mole mass (M), the ideal gas constant (R), and temperature. Here, Vapor pressure (P) is equal to saturated ratio of levoglucosan vapor multiplied saturated levoglucosan vapor pressure at 293.15 K.

S1.2 Calculation of total concentration of generated particles (g/cm³)

$$m_{total} = \frac{dN}{d\log D_p} \times d\log D_p \times \frac{\pi}{6} D_p^3 \times \rho \quad (S3)$$

where dN is particle concentration, D_p is the particle diameter, and ρ is the density of particles.

S1.3 Ratio of the gas-phase concentration to the total concentration of generated particles

$$Ratio = \frac{m_{gas}}{m_{total}} \quad (S4)$$